Fast-scanning two-photon fluorescence imaging based on a microelectromechanical systems two-dimensional scanning mirror

Wibool Piyawattanametha, Robert P. J. Barretto, Tony H. Ko, Benjamin A. Flusberg, and Eric D. Cocker

James H. Clark Center for Biomedical Engineering & Sciences, Stanford University, Stanford, California 94305

Hyejun Ra, Daesung Lee, and Olav Solgaard

Edward L. Ginzton Laboratory, Stanford University, Stanford, California 94305

Mark J. Schnitzer

James H. Clark Center for Biomedical Engineering & Sciences, Stanford University, Stanford, California 94305

Received January 20, 2006; revised March 21, 2006; accepted March 28, 2006; posted April 10, 2006 (Doc. ID 67381)

Towards overcoming the size limitations of conventional two-photon fluorescence microscopy, we introduce two-photon imaging based on microelectromechanical systems (MEMS) scanners. Single crystalline silicon scanning mirrors that are 0.75 mm × 0.75 mm in size and driven in two dimensions by microfabricated vertical comb electrostatic actuators can provide optical deflection angles through a range of ~16°. Using such scanners we demonstrated two-photon microscopy and microendoscopy with fast-axis acquisition rates up to 3.52 kHz.

OCIS codes: 170.2520, 170.2150, 170.5810, 170.3880, 110.2760.

A major focus of current research on two-photon imaging is the development of miniaturized imaging formats, including compact microscopes for handheld imaging, endoscopes for insertion into hollow tissue cavities, and microendoscopes for minimally invasive imaging in solid tissue.[1–7] This goal motivates the creation of miniaturized laser-scanning mechanisms that are compatible with such reduced-size instrumentation.

To date, several miniaturized scanning mechanisms have been explored for confocal and two-photon fluorescence imaging. These are mainly cantilever mechanisms in which a fiber,[1,2,8,9] a small lens,[10] or the two in combination[11] vibrate at resonance. Such mechanisms typically prohibit size reduction below the centimeter scale, restrict the choice of scanning rates, and preclude batch fabrication. What have been missing are millimeter-sized scanners that provide adjustable, rapid line-scanning rates up to ~1 kHz or more, for studying fast biological processes such as blood flow and neuronal activity. Unfortunately, conventional scanners, including galvanometer, spinning polygon, and acousto-optic scanners, cannot be readily miniaturized.

We report the use of microelectromechanical systems (MEMS) scanners for filling this niche for two-photon imaging. Imaging based on MEMS scanners has been demonstrated previously for confocal reflectance[12–14] and optical coherence tomography[15–17] modalities. We fabricated scanners based on electrostatic vertical comb actuators that generally provide greater force and angular range than parallel plate counterparts.[18,19] Comb actuators and a gimbal design allow rotation in two dimensions with minimal mechanical cross talk.[19]

The scanners are batch fabricated on a double silicon-on-insulator wafer that provides an upper device layer 30 μm in thickness, a lower device layer (30 μm), and a substrate (531 μm), which are all single-crystalline silicon. The mirror, movable comb teeth, and inner torsional springs reside in the upper device layer. The frame, outer torsional springs, and fixed comb teeth are fabricated within both device layers. The pronounced thickness of the comb teeth raises the electrostatic torque that can be applied to the mirror, increasing its angular range. Fabrication involves four deep reactive ion-etching steps. The first three steps self-align the comb teeth by transferring mask features sequentially from upper to lower device layers. The last step removes the substrate behind the mirror, releasing the gimbal for rotation.

Using this process, we initially fabricated numerous mirrors that were either 750 μm × 750 μm or 1000 μm × 1000 μm in size, with a range of design values for torsional stiffness and number of comb teeth. We focused our subsequent efforts on a subset of 750 μm × 750 μm mirrors that perform closely to design specifications (Fig. 1). Profilometry studies showed that an uncoated mirror surface has a typical radius of curvature of >1 m and average surface roughness of <16 nm. The die that encompasses each mirror is 3.2 mm × 3.0 mm. The inner and outer torsional springs are 259 μm × 6 μm and 416 μm × 8 μm, respectively (Fig. 1b). There are six banks of comb actuators (Fig. 1c): two that drive the fast, inner rotational axis and four that drive the slower outer axis. In each bank movable and stationary comb teeth are interdigitated and provide electrostatic torque in one direction. The torsional springs supply restoring torque in the opposite direction. These scanners appear to be the smallest used to date for two-photon imaging.

For controlling mirror rotation, the scanner has a ground and four voltage lines, two lines for each axis that control opposing pairs of comb banks (Fig. 1c). Because the torque provided by each bank is propor-

0146-9592/06/132018-3/$15.00

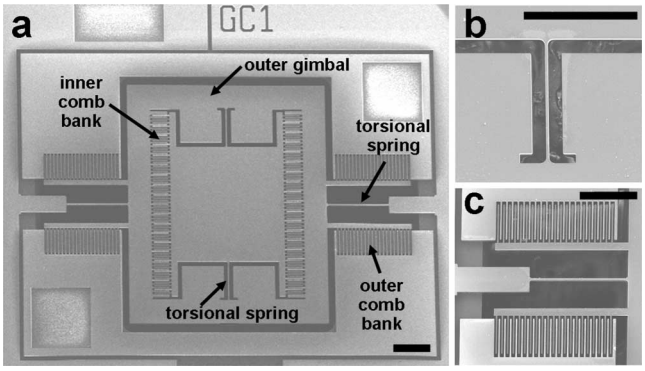

Fig. 1. Electron micrographs of a two-dimensional MEMS scanner. a, 750 μm × 750 μm scanning mirror in a 3.2 mm × 3.0 mm die. Six banks of vertical comb actuators drive the mirror, which has a gimbal design. b, Inner axis torsional spring. c, Outer axis comb bank. Scale bars are 250 μm.

tional to the square of the applied voltage, we drive each pair of banks with voltage signals, $V_1(t)$ and $V_2(t)$, chosen to create a linear relationship between the scan angle and the drive waveform. For $V_1(t) = V_{1,\mathrm{dc}} + V_{\mathrm{ac}} \sin(\omega t)$ and $V_2(t) = V_{2,\mathrm{dc}} + V_{\mathrm{ac}} \sin(\omega t + \pi)$, where $V_{1,\mathrm{dc}}$ and $V_{2,\mathrm{dc}}$ are dc offsets and V_{ac} is the ac voltage amplitude, the net torque provided by a pair of opposing banks is proportional to $[V_1^2(t) - V_2^2(t)]$ and thus to $[V_{1,\mathrm{dc}}^2 - V_{2,\mathrm{dc}}^2 + 2(V_{1,\mathrm{dc}} + V_{2,\mathrm{dc}})V_{\mathrm{ac}} \sin(\omega t)]$. The scanner's range can be centered by adjusting $V_{1,\mathrm{dc}}$ or $V_{2,\mathrm{dc}}$. In pure dc operation, the optical angular ranges for the inner and outer axes are about ±8° and ±3°, respectively (Fig. 2a). In ac mode, the scanning rate can be adjusted from near dc to slightly beyond the mechanically resonant frequencies of 1.76 and 1.02 kHz for the inner and the outer axes, respectively (Fig. 2b). These measured resonant frequencies, f_{res}, are ~6% and ~18% lower, respectively, than expected values based on our design parameters for torsional stiffness, κ (inner axis, 0.68 μN·m; outer axis, 1.44 μN·m), moment of inertia, I (inner axis, 4.9 g·μm^2; outer axis, 25 g·μm^2), and the relationship $2\pi f_{\mathrm{res}} = \sqrt{\kappa/I}$. The discrepancy stems from excess etching.

To test the feasibility of nonlinear optical imaging based on MEMS, we built a tabletop two-photon microscope that employs one of our scanners. When desired, this instrumentation can be additionally equipped with a compound gradient refractive index (GRIN) microendoscope probe for two-photon endoscopy, much as described previously.[3,5] An ultrashort pulsed Ti:sapphire laser provides an excitation beam that is reduced in diameter before reflection off the scanner. The beam is then reexpanded, passes through a dichroic mirror, and fills the back aperture of a microscope objective, which either focuses the light at the specimen plane or into a microendoscope probe that refocuses the light in the sample. In both cases, fluorescence returns back through the objective optics, reflects off the dichroic mirror, and is detected by a photomultiplier tube. Most of our work has relied on uncoated MEMS mirrors that reflect ~35% of the 850 nm laser light, but we have shown mirror metallization can be added to boost reflectance.

We performed raster scanning by driving the mirror with sinusoidal signals from a high-voltage amplifier (AgilOptics). Images were reconstructed based on scanning calibration data obtained by directing the laser beam to a position-sensitive detector (On-Trak). At most drive settings the mirror closely follows the command trajectory. Scan patterns driven by identical signals at 20-min intervals were alike to within <1% and <4% for resonance and off-resonance scanning, respectively. The slight differences mainly represent slight changes in scan amplitude that affect image size calibration but do not produce image distortion.

To demonstrate imaging we studied pollen grain specimens, using two-photon microscopy (Figs. 3a–3c) and microendoscopy (Figs. 3d and 3e). By acquiring data on both the forward and return scanning paths, we achieved a maximal fast-axis acquisition rate of 3.52 kHz, twice the resonant frequency of the inner axis. This is comparable to or faster than rates offered by nonresonant galvanometer scanners. Micrometer-scale details of the pollen are readily apparent in the images (Fig. 3).

One limitation of our system concerns diffraction that occurs for any beam reflecting off the scanner. If such a beam is focused and scanned across the specimen, the maximum number of resolvable focal spots, N, is limited by the ratio of the total angular scanning range, θ_{max}, to the divergence angle, $\delta\theta$, for a beam that overfills the mirror. For a square mirror of width D, the Rayleigh criterion for resolution yields

$$N \cong \frac{\theta_{\mathrm{max}}}{\delta\theta} \cong \frac{\theta_{\mathrm{max}} D}{\lambda},$$

where λ is the wavelength.[20] This bounds the number of distinguishable focal spots in any system based on our scanner to ~250 × 90, given 850 nm light and the measured ranges for the two axes. By comparison, even the smallest single-axis galvanometer scanners

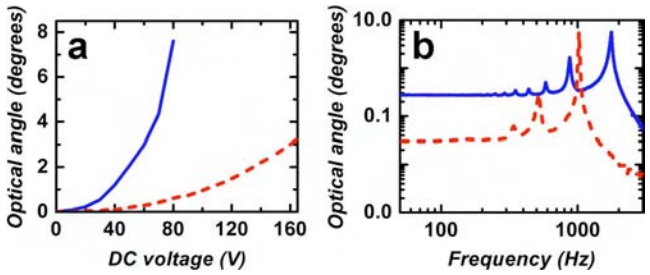

Fig. 2. (Color online) Response characteristics of a 750 μm × 750 μm MEMS scanner. For both a and b, the voltage signal was applied to only one of the two opposing comb banks for each rotational axis. a, Optical deflection angle as a function of dc voltage. The maximum deflection angles are ±7.6° and ±3.0° for the inner (blue solid curve) and outer (red dashed curve) axes, respectively. b, Frequency response functions for the inner (blue solid curve) and outer (red dashed curve) axes, obtained by applying voltage signals of peak-to-peak amplitudes 45 and 58 V to the inner and outer axes, respectively.

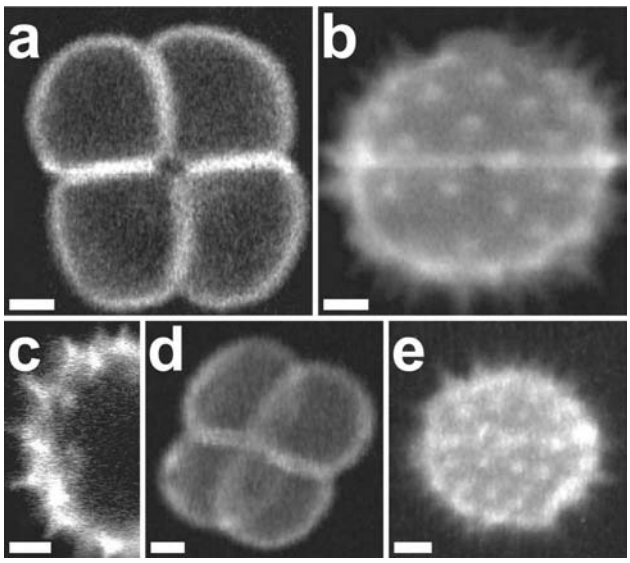

Fig. 3. Two-photon fluorescence images of pollen grains acquired using instrumentation based on a MEMS scanner and a Ti:sapphire laser tuned to 850 nm. a–c, Images acquired using a 40× 0.8 NA water-immersion microscope objective. The fast-axis acquisition rate was 3.2 kHz for a and b and 3.0 kHz for c. Image b is a sum projection from a stack of 38 images acquired at 1 μm increments. d and e, Images acquired using a doublet GRIN microendoscope probe of 0.47 NA and a 10× 0.25 NA microscope objective to couple light into the probe.[3,5] The fast axis was driven at resonance, allowing a double-sided acquisition rate of 3.52 kHz. Image e is a maximum intensity projection from a stack of 46 images acquired at 1 μm increments. Laser power at the sample was 20 mW for a and b, 28 mW for c, and 40 mW for d and e. These power levels were needed because of the fast acquisition rate. Scale bars are 5 μm.

can exhibit $N \sim 5000$. A resonant fiber scanner used for portable two-photon microendoscopy exhibits an N of ~500 or more for each of two axes.[1]

The resolving power of the entire imaging system is set by the product of the optical transfer functions for the scanner and the imaging optics. To balance the competing aims of achieving close to the highest possible resolution over the broadest possible field of view, the contributions of the scanner and imaging optics in setting the resolution limit should be about equal. Given the highest resolution demonstrated with GRIN endoscope probes, ~1 μm,[1,3,5] this criterion yields a field of view of ~250 μm × 90 μm with our current mirror. Future MEMS scanners can achieve modest increases in N over our present design through increases in mirror diameter.

In summary, we have introduced the use of MEMS scanners for two-photon microscopy and microendoscopy, with line acquisition rates up to ~3.5 kHz. We anticipate a broad set of future two-photon imaging applications for such scanners ranging from portable microscopy to minimally invasive endoscopy. Batch fabrication of these scanners will especially aid low-cost applications requiring disposable devices or mass production.

This work was supported by funding to M. Schnitzer from the NSF, NIH, ONR, and the Packard and Beckman Foundations, and by a U54 grant to O. Solgaard from the NCI. B. Flusberg is a NSF Graduate Fellow. E. Cocker is a member of the NIH Stanford Biotechnology Program. Correspondence should be sent to mschnitz@stanford.edu.

Note added in proof: Fu *et al.* have shown two-photon excitation using a single-axis MEMS scanner.[21]

References

1. B. A. Flusberg, J. C. Jung, E. D. Cocker, E. P. Anderson, and M. J. Schnitzer, Opt. Lett. **30**, 2272 (2005).
2. F. Helmchen, M. S. Fee, D. W. Tank, and W. Denk, Neuron **31**, 903 (2001).
3. M. J. Levene, D. A. Dombeck, K. A. Kasischke, R. P. Molloy, and W. W. Webb, J. Neurophysiol. **91**, 1908 (2004).
4. W. Gobel, J. N. Kerr, A. Nimmerjahn, and F. Helmchen, Opt. Lett. **29**, 2521 (2004).
5. J. C. Jung and M. J. Schnitzer, Opt. Lett. **28**, 902 (2003).
6. D. Kim, K. H. Kim, S. Yazdanfar, and P. T. C. So, in Proc. SPIE **5700**, 14 (2005).
7. D. Bird and M. Gu, Opt. Lett. **28**, 1552 (2003).
8. P. M. Delaney and M. R. Harris, in *Handbook of Biological Confocal Microscopy*, 2nd ed., J. B. Pawley, ed. (Plenum, 1995), pp. 515–523.
9. X. Liu, M. J. Cobb, Y. Chen, M. B. Kimmey, and X. Li, Opt. Lett. **29**, 1763 (2004).
10. D. L. Dickensheets and G. S. Kino, in Proc. SPIE **2184**, 39 (1994).
11. L. Giniunas, R. Juskaitis, and S. V. Shatalin, J. Opt. Soc. Am. A **27**, 724 (1991).
12. D. L. Dickensheets and G. S. Kino, Opt. Lett. **21**, 764 (1996).
13. W. Piyawattanametha, H. Toshiyoshi, J. LaCosse, and M. C. Wu, in *Conference on Lasers and Electro-Optics (CLEO 2000)*, Vol. 39 of OSA Trends in Optics and Photonics (Optical Society of America, 2000), pp. 447–448.
14. U. Hofmann, S. Muehlmann, M. Witt, K. Dorschel, R. Schutz, and B. Wagner, presented at the Miniaturized Systems with Micro-Optics and MEMS meeting, Santa Clara, Calif., 1999.
15. J. M. Zara, S. Yazdanfar, K. D. Rao, J. A. Izatt, and S. W. Smith, Opt. Lett. **28**, 628 (2003).
16. W. Piyawattanametha, L. Fan, S. Hsu, M. Fujino, M. C. Wu, P. R. Herz, A. D. Aguirre, Y. Chen, and J. G. Fujimoto, in *Conference on Lasers and Electro-Optics (CLEO)* (Optical Society of America, 2004), paper CWS2.
17. Y. Pan, H. Xie, and G. K. Fedder, Opt. Lett. **26**, 1966 (2001).
18. W. Piyawattanametha, P. R. Patterson, D. Hah, H. Toshiyoshi, and M. C. Wu, J. Microelectromech. Syst. **14**, 1329 (2005).
19. D. Lee and O. Solgaard, in *Proceedings of the Solid-State Sensor and Actuator Workshop*, Hilton Head, South Carolina, June 6–10, 2004, pp 352–355.
20. M. Born and E. Wolf, *Principles of Optics*, 7th ed. (Cambridge U. Press, 1999), p. 949.
21. L. Fu, A. Jain, H. Xie, C. Cranfield, and M. Gu, Opt. Express **14**, 1027 (2006).